

Title: Soil-respiration driven CO₂ pulses dominate Australia's flux variability

Authors: Eva-Marie Metz^{1*}, Sanam N. Vardag^{1,2}, Sourish Basu^{3,4}, Martin Jung⁵, Bernhard Ahrens⁵, Tarek El-Madany⁵, Stephen Sitch⁶, Vivek K. Arora⁷, Peter R. Briggs⁸, Pierre Friedlingstein^{9,10}, Daniel S. Goll¹¹, Atul K. Jain¹², Etsushi Kato¹³, Danica Lombardozzi¹⁴, Julia E.M.S. Nabel^{5,15}, Benjamin Poulter¹⁶, Roland Séférian¹⁷, Hanqin Tian¹⁸, Andrew Wiltshire¹⁹, Wenping Yuan²⁰, Xu Yue²¹, Sönke Zaehle⁵, Nicholas M. Deutscher²², David W.T. Griffith²² and André Butz^{1,2,23*}

Affiliations:

¹Institute of Environmental Physics, Heidelberg University; Im Neuenheimer Feld 229, Heidelberg, 69120, Germany.

²Heidelberg Center for the Environment (HCE), Heidelberg University; Im Neuenheimer Feld, 130.1, Heidelberg, 69120, Germany.

³Goddard Space Flight Center, NASA; 8800 Greenbelt Rd, Greenbelt, 20771, Maryland, USA.

⁴Earth System Science Interdisciplinary Center, University of Maryland; 5825 University Research Court, Suite 4001, College Park, 20740, Maryland, USA.

⁵Max Planck Institute for Biogeochemistry; Hans-Knöll-Straße 10, Jena, 07745, Germany.

⁶College of Life and Environmental Sciences, University of Exeter; North Park Road, Exeter, EX4 4RJ, Devon, UK.

⁷Canadian Centre for Climate Modelling and Analysis, Environment and Climate Change Canada; 200-2474 Arbutus Road, Victoria, B.C., V8N 1V9, Canada.

⁸Climate Science Centre, CSIRO Oceans and Atmosphere; Canberra, ACT 2601, Australia.

⁹College of Engineering, Mathematics and Physical Sciences, University of Exeter; Exeter EX4 4QF, United Kingdom.

¹⁰Laboratoire de Météorologie Dynamique, Institut Pierre-Simon Laplace, CNRS-ENS-UPMC-X, Département de Géosciences, Ecole Normale Supérieure; 24 rue Lhomond, 75005 Paris, France.

¹¹Université Paris Saclay, CEA-CNRS-UVSQ, LSCE/IPSL; Gif sur Yvette, France.

¹²Department of Atmospheric Sciences, University of Illinois; Urbana, IL 61801, USA.

¹³Institute of Applied Energy; Tokyo 105-0003, Japan.

¹⁴Climate and Global Dynamics Laboratory, National Center for Atmospheric Research; 1850 Table Mesa Drive Boulder, CO 80305, USA

¹⁵Max Planck Institute for Meteorology; Bundesstr. 53, 20146 Hamburg, Germany.

¹⁶Biospheric Sciences Laboratory, Goddard Space Flight Center, NASA; Greenbelt, 20771, Maryland, USA.

¹⁷CNRM, Université de Toulouse, Météo-France, CNRS; Toulouse, France.

¹⁸International Center for Climate and Global Change Research, School of Forestry and Wildlife Sciences, Auburn University; AL 36849, USA.

¹⁹Met Office Hadley Centre; FitzRoy Road, Exeter EX1 3PB, UK.

²⁰School of Atmospheric Sciences, Southern Marine Science and Engineering Guangdong Laboratory (Zhuhai), Sun Yat-sen University; Zhuhai 519082, China.

5 ²¹School of Environmental Science and Engineering, Nanjing University of Information Science & Technology (NUIST); Nanjing 210044, China.

²²Centre for Atmospheric Chemistry, School of Chemistry, University of Wollongong; Wollongong, NSW, 2522, Australia.

²³Interdisciplinary Center for Scientific Computing (IWR), Heidelberg University; Im Neuenheimer Feld, 205, Heidelberg, 69120, Germany.

10 *Corresponding author. Email: eschoema@iup.uni-heidelberg.de, andre.butz@iup.uni-heidelberg.de

Abstract: The Australian continent contributes substantially to the year-to-year variability of the global terrestrial carbon dioxide (CO₂) sink. However, the scarcity of in-situ observations in remote areas prevents deciphering the processes that force the CO₂ flux variability. Here, examining atmospheric CO₂ measurements from satellites in the period 2009-2018, we find recurrent end-of-dry-season CO₂ pulses over the Australian continent. These pulses largely control the year-to-year variability of Australia's CO₂ balance, due to 2-3 times higher seasonal variations compared to previous top-down inversions and bottom-up estimates. The pulses occur shortly after the onset of rainfall and are driven by enhanced soil-respiration preceding photosynthetic uptake in Australia's semi-arid regions. The suggested continental-scale relevance of soil-rewetting processes has large implications for our understanding and modelling of global climate-carbon cycle feedbacks.

20 **One Sentence Summary:** Satellite CO₂ measurements find large CO₂ pulses over Australia attributable to rewetting of seasonally dry soils.

Terrestrial ecosystems drive the seasonal and year-to-year variability of the global carbon dioxide (CO₂) sink (1). Previous research identified semi-arid regions as hotspots of global CO₂ balance inter-annual variability (2–5) due to their large sensitivity of photosynthetic carbon uptake to fluctuations in water availability (6, 7). The Australian continent is primarily covered with semi-arid ecosystems and experiences large variations in rainfall. This makes Australia particularly relevant for the variability in the global carbon cycle (8–13), contributing up to 60% to yearly anomalies of the global terrestrial CO₂ sink (2).

However, current approaches for attributing global CO₂ sink variations to certain regions and mechanisms are highly uncertain, which limits our ability to model climate-carbon cycle feedbacks and project future climate (14, 15). Global process-based ecosystem models underestimate observed CO₂ flux variability across semi-arid sites due to the complexity of carbon-water cycle interactions and the diversity of ecosystem responses to water fluctuations (16, 17). The same holds true for machine learning based models trained on local carbon flux observations (18, 19), which is due to the scarcity of available flux measurements in low-latitude semi-arid regions (20) as well as due to the inability to represent potentially important non-instantaneous carry-over effects (21). Atmospheric transport inversions based on in-situ measurements of airborne CO₂ also suffer from the scarcity of observations in remote areas and thus the inversions cannot reliably attribute CO₂ flux variability to specific regions, despite growing monitoring capacities (22, 23). However, recent satellite observations of atmospheric column CO₂ deliver data where ground-based in-situ concentration measurements and carbon flux networks are sparse and thus, satellite CO₂ data can fill important gaps and provide new constraints on regional scale patterns and processes (8, 24–28).

Here, using satellite observations of atmospheric CO₂ concentrations from the Greenhouse Gases Observing Satellite (GOSAT) for the period 2009 to 2018, we identify a net CO₂ pulse to

the atmosphere that occurs over Australia at the end of the dry season in most years with variable magnitude. We show that this pattern appears to dominate the seasonal and year-to-year variations of Australia's CO₂ balance for that period, while it is not evident in traditional atmospheric inversions using in-situ measurements only, in the FLUXCOM machine learning based extrapolations of in-situ flux measurements (18, 20), and most process-based ecosystem models of the TRENDY initiative (42). The few process-based TRENDY models that reproduce the CO₂ pulse pattern qualitatively suggest that it is caused by rapid respiratory carbon release with the onset of the rainy season while the increase in photosynthetic carbon uptake lags behind. This observed process is consistent with the phenomenon of respiration pulses after rewetting events discussed in the context of the "Birch effect" (29, 30). Such pulses have been described extensively in local studies of water-limited systems (31) but their large-scale relevance remained unknown.

Atmospheric CO₂ peak over Australia

The Greenhouse Gases Observing Satellite (GOSAT) has been delivering global measurements of the column-average dry-air mole fractions ("concentrations") of atmospheric CO₂ since its launch in 2009 (32). After subtracting the secular trend (33), the record of GOSAT concentrations for the period 2009-2018 (Fig. 1) reveals a seasonal pattern above Australia with CO₂ draw-down in March, April, May (MAM) and a CO₂ peak of variable magnitude at the end of the dry season in October, November, December (OND). These patterns are consistent among two retrievals independently applied to GOSAT (GOSAT/RemoTeC (34) and GOSAT/ACOS (35), Table S1) and they are present in CO₂ concentrations measured by the Orbiting Carbon Observatory (OCO-2 (36, 37), period 2015 to 2018, Table S1) as well as in ground-based data of the Total Carbon Column Observing Network (38) (Fig. S1 and S2).

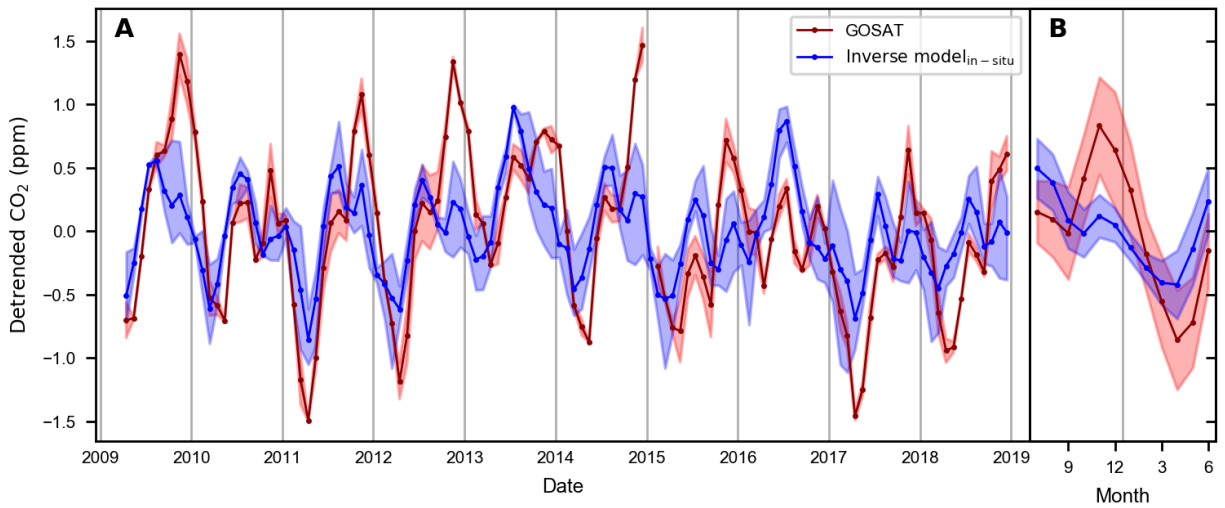


Fig. 1. Detrended CO₂ concentrations over Australia from satellite and models. (A)

Detrended column-average dry-air mole fractions of CO₂ measured by GOSAT (red) and
5 simulated by inverse models assimilating in-situ ground-based measurements (blue). Data are
monthly averages for Australia. Red shading indicates the range of the GOSAT/RemoTeC and
GOSAT/ACOS algorithms. Blue shading indicates the range of the CarbonTracker, CAMS, and
TM5-4DVAR inverse models. **(B)** Mean and standard deviation (shading) over the period 2009
to 2018.

10
In contrast, the atmospheric column CO₂ concentrations simulated by three inverse atmospheric
transport models (CarbonTracker CT2019B (39), CAMS (40), TM5-4DVAR (41)) underestimate
the CO₂ draw-down in MAM and lack the CO₂ pulses in OND (Fig. 1). Driven by atmospheric
winds, these transport models deliver concentration fields that are optimally compatible with in-
15 situ measured CO₂ concentrations and the a priori biogenic, oceanic, fire and fossil CO₂ surface-
atmosphere fluxes (33). However, due to their sparsity in and around Australia (see Fig. S3
compared to Fig. S4), the in-situ measurements provide only marginal constraints on the regional
flux balance. Thus, the discrepancy between CO₂ concentrations from GOSAT and traditional in-

in situ based atmospheric inversions hints at the existence of a carbon release mechanism in Australian ecosystems that has remained undetected by the existing in-situ CO₂ monitoring system.

5 **Australian top-down and bottom-up fluxes**

To improve on the surface flux estimates for Australia, we feed the GOSAT CO₂ concentrations into one of the atmospheric inverse models (TM5-4DVAR) together with the in-situ CO₂ measurements. We find indeed that the recurring end-of-dry-season CO₂ concentration peaks are attributed to a carbon release pattern originating from land ecosystems, which is not present in the inversions when assimilating in-situ CO₂ data alone (Fig. 2A and Fig. S5).

Our new estimates of Australia's carbon balance variability based on assimilating GOSAT together with in-situ data show a nearly doubled peak-to-peak amplitude of the seasonal cycle (174±40 TgC/month, mean ± standard deviation over the 2009 to 2018 period, July-to-June peak-to-peak amplitude) compared to the in-situ-only inversions (88±13 TgC/month). Moreover, the end-of-dry-season CO₂ pulses found by the GOSAT inversions imply a more than 4-fold greater year-to-year variability of the annual CO₂ fluxes (0.207 PgC/a, standard deviation over the 2010 to 2018 period) than for the in-situ-only inversions (0.039 PgC/a) (Fig. S7 and Table S2). Fluxes obtained by assimilating OCO-2 together with in-situ data for the period 2015 to 2018 show the same end-of-dry-season pulses and agree well with the fluxes of the GOSAT inversion (see Fig. S6).

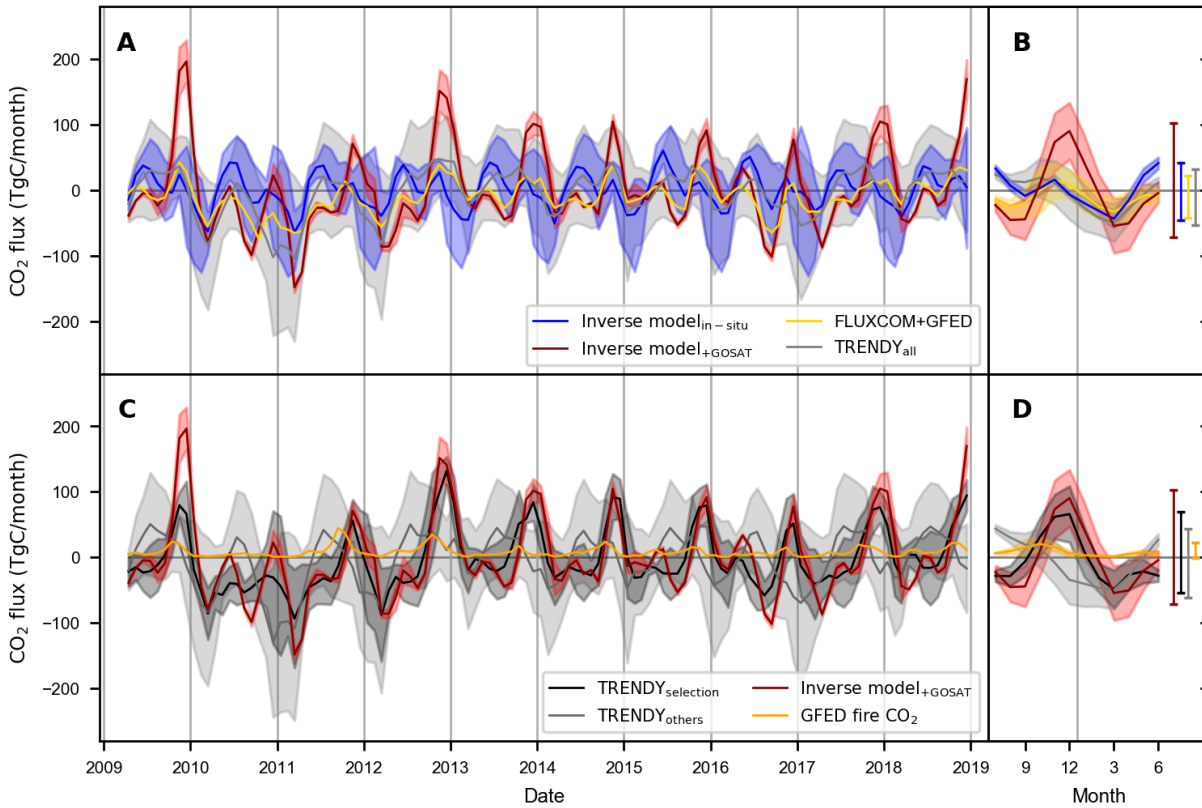


Fig. 2. Australian net CO₂ fluxes. (A) Top-down estimates of the net monthly Australian carbon fluxes inferred by in-situ CO₂ measurements based inverse models (blue) and by TM5-4DVAR assimilating in-situ measurements together with GOSAT observations (red), compared to bottom-up FLUXCOM+GFED NBP (yellow) and the TRENDY ensemble mean NBP (grey). Shading indicates the range among the various top-down data streams (in-situ based CarbonTracker, CAMS, and TM5-4DVAR in blue, TM5-4DVAR_{+RemoTeC/GOSAT} and TM5-4DVAR_{+ACOS/GOSAT} in red) and the standard deviation among the TRENDY ensemble (grey). (C) NBP of a subgroup of TRENDY models (black) compared to the other models (grey), to the GOSAT inversions (red, same as in (A)) and to GFED fire emissions (orange). Shading as in (A). (B) and (D) Mean and standard deviation (shading) over the period 2009 to 2018 and the mean peak-to-peak seasonal cycle amplitudes (bars). Positive fluxes correspond to carbon emissions into the atmosphere.

To understand the origin of the CO₂ pulses, we compare to bottom-up estimates from machine learning (FLUXCOM (18, 20)) and 18 process-based dynamic global vegetation models (DGVMs) from the TRENDY (v9) ensemble (42). Those also provide the component fluxes of gross primary productivity (GPP) and terrestrial ecosystem respiration (TER) enabling the attribution to variations in photosynthetic carbon uptake and respiratory carbon release. We further include fire emissions (FIRE) from the Global Fire Emission Database (GFED) as a potential factor for explaining the pattern. To compare to the top-down inversions, we calculate net biome production ($NBP = TER + FIRE - GPP$) by adding fire emissions from GFED to net ecosystem exchange ($NEE = TER - GPP$) from FLUXCOM. That is, positive fluxes correspond to carbon emissions into the atmosphere. For TRENDY, NBP is taken directly from the simulations of the DGVMs. We find that FLUXCOM+GFED derived NBP lacks the end-of-dry-season CO₂ pulses (Fig. 2A) and its seasonal amplitude (64 ± 16 TgC/month) underestimates the one found by the GOSAT inversions by a factor of 3. This could be explained by the sparsity of Australian flux tower data in the training of the FLUXCOM machine learning models (only 4 of 224 sites lie in Australia, see Fig. S3) causing extrapolation errors (18), and by known weaknesses in representing certain fluctuations in response to water availability (19) or “memory” effects due to non-accounted carbon pool dynamics (43). Our analysis further suggests that local and transported fire emissions might contribute at the beginning of the carbon pulses but cannot explain their magnitude and duration (Fig. 2B and Fig. S8).

The ensemble of TRENDY NBP simulations shows a large inter-model spread and also no end-of-dry-season CO₂ pulses on average (Fig. 2A) causing a seasonal amplitude (85 ± 20 TgC/month) which is about half of that of the GOSAT inversions. However, the dry season pulses are present in a subset of five of the TRENDY DGVMs (Fig. 2B and Table S1). For this

subset, the timing, the duration and the magnitude (except for the year 2009) of the pulses and their seasonal amplitude (123 ± 31 TgC/month) are closer to the pulses found by the GOSAT inversions. This finding suggests that the CO₂ pulses can be explained by ecosystem processes shaping the phasing of photosynthesis and respiration.

5

Phasing of respiration and photosynthesis

We find that the subset of DGVMs which are in good agreement with the GOSAT inversions reveals a distinctly different seasonal timing of GPP and TER than the other DGVMs. For the selected subset, the CO₂ pulses are driven by TER, which increases rapidly at the onset of the rainy season while GPP takes up only a few weeks later (Fig. 3A). The pulses originate mainly from an early increase of soil-respiration in semi-arid regions (Fig. S9, Fig. S10A). For the other DGVMs, TER and GPP show a mostly synchronous phasing throughout the year yielding no CO₂ pulses (Fig. 3B and Fig. S10B). The precipitation records for the semi-arid regions of Australia (Fig. 3C, Fig. S3) suggest that the soil-respiration driven pulses shown by the GOSAT inversions and the selected TRENDY models are weaker or do not occur in years with anomalously strong precipitation during the dry period (Austral winter) such as in the La Nina years 2010 and 2016. This implies that the observed pulses are conditional on rewetting of dry soils and that it is through the strength of the pulses that climatic conditions have control on Australia's annual CO₂ balance (Fig. S7)

10

15

20

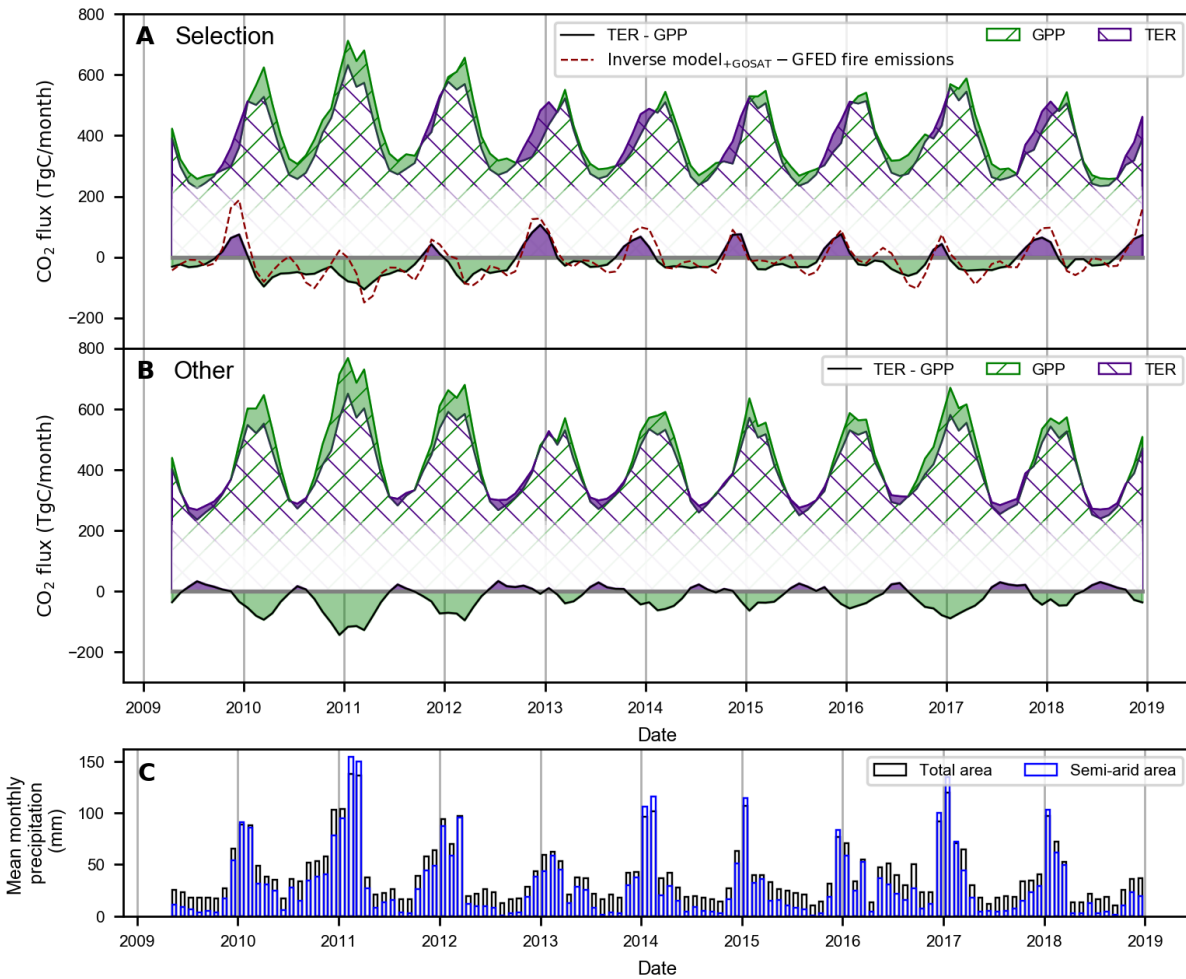


Fig. 3. Seasonal timing of gross carbon fluxes among TRENDY models. (A) Gross primary production (GPP, green) and total respiration (TER, purple) for Australia for the selection of TRENDY DGVMs that replicate the end-of-dry-season CO₂ pulses. The difference of TER and GPP is given in black in the lower part together with GOSAT-based inversion where GFED fire emissions are subtracted (dashed red). **(B)** Same as panel a but for the other TRENDY models that do not replicate the end-of-dry-season CO₂ pulses. **(C)** Mean monthly precipitation over the entire Australian region (black) and the semi-arid part (see Fig. S3) of Australia (blue).

10 The detected continental-scale CO₂ pulses are consistent with site-level observations of dryland ecosystems which show an asynchronous response of respiration and photosynthesis to

precipitation pulses (44). The rapid response of microbial respiration to rewetting events, is known as “Birch effect” and has been described in the literature of specific sites in some semi-arid regions for many decades (29–31). After being dormant in the dry period, soil microbes are activated by the moisture supply from rainfall. Benefitting from warm soils, accumulated and readily available substrate gets respired quickly going along with rapid growth of microbial populations. These dynamics of soil microbial processes cause respiration CO₂ pulses with rewetting of dry soils which are evident in Australian flux tower data (Fig. S11 and S12).

Photodegradation of surface litter (45) and the death of microorganisms during the dry period (46, 47) may lead to the accumulation of easily decomposable substrate available to microorganisms at the onset of rain. It remains an open question whether the respiration pulses are mainly driven by substrates accumulated during the dry period and to what extent they are fueled by mobilization and decomposition of physically protected carbon (47). These processes are not represented explicitly or in detail in the TRENDY DGVMs and thus, the DGVMs cannot resolve how the site-level mechanisms scale up to the continental-scale effect observed here.

Nonetheless, a selection of models effectively captures the continental-scale CO₂ pulses by a fast response of respiration and a delayed response of photosynthesis to the onset of the rainy season. This highlights the importance of subtle differences in effective parameterizations of respiration and photosynthesis to moisture fluctuations. Associated uncertainties affect the skill of the models to represent the carbon cycle of semi-arid ecosystems.

Our study demonstrates that the soil-respiration driven CO₂ pulses over Australia following the end of the dry season are of large-scale relevance and appear to dominate the variability of the continent’s carbon balance. The GOSAT inversions have shed light on a blind spot of previous top-down and bottom-up approaches for quantifying and attributing CO₂ flux variability. This is important since Australia’s semi-arid regions contribute largely to the IAV of the global terrestrial

carbon sink and since it is the ecosystem response to the phasing of dry and wet periods that drives the seasonal mechanism behind the large IAV. Thus, our study calls for revisiting the contributions of global semi-arid systems to CO₂ balance variations and for assessing implications for our ability to model climate-carbon feedbacks in semi-arid regions. Only a few of the global vegetation models are able to reproduce the observed CO₂ pulses which suggests that only their respective parameterizations are able to represent the sensitivity of the underlying mechanism to changes in climatic conditions and thus, to accurately project semi-arid carbon flux variability under a changing climate. Considering the large uncertainties associated with modeling climate-carbon feedbacks (14,15,X), our findings may contribute continental-scale mechanistic understanding that can help reduce these uncertainties for dryland ecosystems which are found particularly sensitive to climate change (X).

References and Notes

1. P. Friedlingstein, M. O'sullivan, M. W. Jones, R. M. Andrew, J. Hauck, A. Olsen, G. P. Peters, W. Peters, J. Pongratz, S. Sitch, C. Le Quéré, J. G. Canadell, P. Ciais, R. B. Jackson, S. Alin, Aragão, Luiz E. O. C., A. Arneeth, V. Arora, N. R. Bates, M. Becker, A. Benoit-Cattin, H. C. Bittig, L. Bopp, S. Bultan, N. Chandra, F. Chevallier, L. P. Chini, W. Evans, L. Florentie, P. M. Forster, T. Gasser, M. Gehlen, D. Gilfillan, T. Gkritzalis, L. Gregor, N. Gruber, I. Harris, K. Hartung, V. Haverd, R. A. Houghton, T. Ilyina, A. K. Jain, E. Joetzjer, K. Kadono, E. Kato, V. Kitidis, J. I. Korsbakken, P. Landschützer, N. Lefèvre, A. Lenton, S. Lienert, Z. Liu, D. Lombardozzi, G. Marland, N. Metzler, D. R. Munro, Nabel, Julia E. M. S., S.-I. Nakaoka, Y. Niwa, K. O'Brien, T. Ono, P. I. Palmer, D. Pierrot, B. Poulter, L. Resplandy, E. Robertson, C. Rödenbeck, J. Schwinger, R. Séférian, I. Skjelvan, A. J. P. Smith, A. J. Sutton, T. Tanhua, P. P. Tans, H. Tian, B. Tilbrook, G. van der Werf, N. Vuichard, A. P. Walker, R. Wanninkhof, A. J. Watson, D. Willis, A. J. Wiltshire, W. Yuan,

X. Yue, S. Zaehle, Global Carbon Budget 2020. *Earth Syst. Sci. Data.* **12**, 3269–3340 (2020), doi:10.5194/essd-12-3269-2020.

2. B. Poulter, D. Frank, P. Ciais, R. B. Myneni, N. Andela, J. Bi, G. Broquet, J. G. Canadell, F. Chevallier, Y. Y. Liu, S. W. Running, S. Sitch, G. R. van der Werf, Contribution of semi-arid ecosystems to interannual variability of the global carbon cycle. *Nature.* **509**, 600–603
5 (2014), doi:10.1038/nature13376.

3. A. Ahlström, M. R. Raupach, G. Schurgers, B. Smith, A. Arneeth, M. Jung, M. Reichstein, J. G. Canadell, P. Friedlingstein, A. K. Jain, others, The dominant role of semi-arid ecosystems in the trend and variability of the land CO₂ sink. *Science.* **348**, 895–899 (2015).

10 4. M. Jung, M. Reichstein, C. R. Schwalm, C. Huntingford, S. Sitch, A. Ahlström, A. Arneeth, G. Camps-Valls, P. Ciais, P. Friedlingstein, F. Gans, K. Ichii, A. K. Jain, E. Kato, D. Papale, B. Poulter, B. Raduly, C. Rödenbeck, G. Tramontana, N. Viovy, Y.-P. Wang, U. Weber, S. Zaehle, N. Zeng, Compensatory water effects link yearly global land CO₂ sink changes to temperature. *Nature.* **541**, 516–520 (2017), doi:10.1038/nature20780.

15 5. V. Humphrey, A. Berg, P. Ciais, P. Gentine, M. Jung, M. Reichstein, S. I. Seneviratne, C. Frankenberg, Soil moisture-atmosphere feedback dominates land carbon uptake variability. *Nature.* **592**, 65–69 (2021).

6. S. Piao, X. Wang, K. Wang, X. Li, A. Bastos, J. G. Canadell, P. Ciais, P. Friedlingstein, S. Sitch, Interannual variation of terrestrial carbon cycle: Issues and perspectives. *Glob Change Biol.* **26**, 300–318 (2020), doi:10.1111/gcb.14884.

20 7. V. Haverd, A. Ahlström, B. Smith, J. G. Canadell, Carbon cycle responses of semi-arid ecosystems to positive asymmetry in rainfall. *Glob Change Biol.* **23**, 793–800 (2017), doi:10.1111/gcb.13412.

8. R. G. Detmers, O. Hasekamp, I. Aben, S. Houweling, T. T. Leeuwen, A. Butz, J. Landgraf, P. Köhler, L. Guanter, B. Poulter, Anomalous carbon uptake in Australia as seen by GOSAT. *Geophys. Res. Lett.* **42**, 8177–8184 (2015), doi:10.1002/2015GL065161.
9. X. Ma, A. Huete, J. Cleverly, D. Eamus, F. Chevallier, J. Joiner, B. Poulter, Y. Zhang, L. Guanter, W. Meyer, Z. Xie, G. Ponce-Campos, Drought rapidly diminishes the large net CO₂ uptake in 2011 over semi-arid Australia. *Sci. Rep.* **6**, 37747 (2016), doi:10.1038/srep37747.
10. J. Cleverly, D. Eamus, Q. Luo, N. Restrepo Coupe, N. Kljun, X. Ma, C. Ewenz, L. Li, Q. Yu, A. Huete, The importance of interacting climate modes on Australia’s contribution to global carbon cycle extremes. *Sci. Rep.* **6**, 23113 (2016), doi:10.1038/srep23113.
11. Z. Xie, A. Huete, J. Cleverly, S. Phinn, E. McDonald-Madden, Y. Cao, F. Qin, Multi-climate mode interactions drive hydrological and vegetation responses to hydroclimatic extremes in Australia. *Remote Sensing of Environment.* **231**, 111270 (2019), doi:10.1016/j.rse.2019.111270.
12. A. Bastos, M. O’Sullivan, P. Ciais, D. Makowski, S. Sitch, P. Friedlingstein, F. Chevallier, C. Rödenbeck, J. Pongratz, I. T. Lujikx, others, Sources of uncertainty in regional and global terrestrial CO₂ exchange estimates. *Global Biogeochemical Cycles.* **34**, e2019GB006393 (2020).
13. L. Teckentrup, M. G. de Kauwe, A. J. Pitman, D. S. Goll, V. Haverd, A. K. Jain, E. Joetzjer, E. Kato, S. Lienert, D. Lombardozzi, others, Assessing the representation of the Australian carbon cycle in global vegetation models. *Biogeosciences.* **18**, 5639–5668 (2021).
14. P. M. Cox, C. Huntingford, M. S. Williamson, Emergent constraint on equilibrium climate sensitivity from global temperature variability. *Nature.* **553**, 319–322 (2018), doi:10.1038/nature25450.

15. S. Wenzel, P. M. Cox, V. Eyring, P. Friedlingstein, Projected land photosynthesis constrained by changes in the seasonal cycle of atmospheric CO₂. *Nature*. **538**, 499–501 (2016), doi:10.1038/nature19772.
16. D. L. Hoover, A. A. Pfennigwerth, M. C. Duniway, Drought resistance and resilience: The role of soil moisture–plant interactions and legacies in a dryland ecosystem. *J. Ecol. (Journal of Ecology)*. **109**, 3280–3294 (2021), doi:10.1111/1365-2745.13681.
17. N. MacBean, R. L. Scott, J. A. Biederman, P. Peylin, T. Kolb, M. E. Litvak, P. Krishnan, T. P. Meyers, V. K. Arora, V. Bastrikov, D. Goll, D. L. Lombardozzi, Nabel, Julia E. M. S., J. Pongratz, S. Sitch, A. P. Walker, S. Zaehle, D. J. P. Moore, Dynamic global vegetation models underestimate net CO₂ flux mean and inter-annual variability in dryland ecosystems. *Environ. Res. Lett.* **16**, 94023 (2021), doi:10.1088/1748-9326/ac1a38.
18. G. Tramontana, M. Jung, C. R. Schwalm, K. Ichii, G. Camps-Valls, B. Ráduly, M. Reichstein, M. A. Arain, A. Cescatti, G. Kiely, others, Predicting carbon dioxide and energy fluxes across global FLUXNET sites with regression algorithms. *Biogeosciences*. **13**, 4291–4313 (2016).
19. P. Bodesheim, M. Jung, F. Gans, M. D. Mahecha, M. Reichstein, Upscaled diurnal cycles of land–atmosphere fluxes: a new global half-hourly data product. *Earth Syst. Sci. Data*. **10**, 1327–1365 (2018), doi:10.5194/essd-10-1327-2018.
20. M. Jung, C. Schwalm, M. Migliavacca, S. Walther, G. Camps-Valls, S. Koirala, P. Anthoni, S. Besnard, P. Bodesheim, N. Carvalhais, others, Scaling carbon fluxes from eddy covariance sites to globe: synthesis and evaluation of the FLUXCOM approach. *Biogeosciences*. **17**, 1343–1365 (2020).

21. S. Sippel, M. Reichstein, X. Ma, M. D. Mahecha, H. Lange, M. Flach, D. Frank, Drought, Heat, and the Carbon Cycle: a Review. *Curr. Clim. Change Rep.* **4**, 266–286 (2018), doi:10.1007/s40641-018-0103-4.
22. J. Beringer, L. B. Hutley, I. McHugh, S. K. Arndt, D. Campbell, H. A. Cleugh, J. Cleverly, V. Resco de Dios, D. Eamus, B. Evans, C. Ewenz, P. Grace, A. Griebel, V. Haverd, N. Hinko-Najera, A. Huete, P. Isaac, K. Kanniah, R. Leuning, M. J. Liddell, C. Macfarlane, W. Meyer, C. Moore, E. Pendall, A. Phillips, R. L. Phillips, S. M. Prober, N. Restrepo-Coupe, S. Rutledge, I. Schroder, R. Silberstein, P. Southall, M. S. Yee, N. J. Tapper, E. van Gorsel, C. Vote, J. Walker, T. Wardlaw, An introduction to the Australian and New Zealand flux tower network –OzFlux. *Biogeosciences*. **13**, 5895–5916 (2016), doi:10.5194/bg-13-5895-2016.
23. J. Cleverly, D. Eamus, W. Edwards, M. Grant, M. J. Grundy, A. Held, M. Karan, A. J. Lowe, S. M. Prober, B. Sparrow, B. Morris, TERN, Australia’s land observatory: addressing the global challenge of forecasting ecosystem responses to climate variability and change. *Environ. Res. Lett.* **14**, 95004 (2019), doi:10.1088/1748-9326/ab33cb.
24. P. J. Sellers, D. S. Schimel, B. Moore, J. Liu, A. Eldering, Observing carbon cycle–climate feedbacks from space. *Proc. Natl. Acad. Sci. USA*. **115**, 7860–7868 (2018), doi:10.1073/pnas.1716613115.
25. P. I. Palmer, L. Feng, D. Baker, F. Chevallier, H. Bösch, P. Somkuti, Net carbon emissions from African biosphere dominate pan-tropical atmospheric CO₂ signal. *Nature communications*. **10**, 1–9 (2019).
26. B. Byrne, J. Liu, M. Lee, I. Baker, K. W. Bowman, N. M. Deutscher, D. G. Feist, D. W. T. Griffith, L. T. Iraci, M. Kiel, J. S. Kimball, C. E. Miller, I. Morino, N. C. Parazoo, C. Petri, C. M. Roehl, M. K. Sha, K. Strong, V. A. Velazco, P. O. Wennberg, D. Wunch, Improved Constraints on Northern Extratropical CO₂ Fluxes Obtained by Combining Surface-Based and

Space-Based Atmospheric CO₂ Measurements. *J. Geophys. Res. Atmos.* **125** (2020),
doi:10.1029/2019JD032029.

27. Z. Chen, D. N. Huntzinger, J. Liu, S. Piao, X. Wang, S. Sitch, P. Friedlingstein, P. Anthoni,
A. Arneeth, V. Bastrikov, D. S. Goll, V. Haverd, A. K. Jain, E. Joetzjer, E. Kato, S. Lienert, D.
5 L. Lombardozzi, P. C. McGuire, J. R. Melton, Nabel, Julia E M S, J. Pongratz, B. Poulter, H.
Tian, A. J. Wiltshire, S. Zaehle, S. M. Miller, Five years of variability in the global carbon
cycle: comparing an estimate from the Orbiting Carbon Observatory-2 and process-based
models. *Environ. Res. Lett.* **16**, 54041 (2021), doi:10.1088/1748-9326/abfac1.

28. Y. Villalobos, P. Rayner, S. Thomas, J. Silver, The potential of Orbiting Carbon
10 Observatory-2 data to reduce the uncertainties in CO₂ surface fluxes over Australia using a
variational assimilation scheme. *Atmos. Chem. Phys.* **20**, 8473–8500 (2020),
doi:10.5194/acp-20-8473-2020.

29. H. F. Birch, Mineralisation of plant nitrogen following alternate wet and dry conditions.
Plant Soil. **20**, 43–49 (1964), doi:10.1007/bf01378096.

15 30. P. Jarvis, A. Rey, C. Petsikos, L. Wingate, M. Rayment, J. Pereira, J. Banza, J. David, F.
Miglietta, M. Borghetti, G. Manca, R. Valentini, Drying and wetting of Mediterranean soils
stimulates decomposition and carbon dioxide emission: the “Birch effect”. *Tree Physiol.*
(Tree Physiology). **27**, 929–940 (2007), doi:10.1093/treephys/27.7.929.

31. P. Casals, L. Lopez-Sangil, A. Carrara, C. Gimeno, S. Nogués, Autotrophic and heterotrophic
20 contributions to short-term soil CO₂ efflux following simulated summer precipitation pulses
in a Mediterranean dehesa. *Global Biogeochem. Cycles.* **25**, n/a-n/a (2011),
doi:10.1029/2010GB003973.

32. A. Kuze, H. Suto, K. Shiomi, S. Kawakami, M. Tanaka, Y. Ueda, A. Deguchi, J. Yoshida, Y.
Yamamoto, F. Kataoka, T. E. Taylor, H. L. Buijs, Update on GOSAT TANSO-FTS

performance, operations, and data products after more than 6 years in space. *Atmos. Meas. Tech.* **9**, 2445–2461 (2016), doi:10.5194/amt-9-2445-2016.

33. *Materials and methods are available as supplementary materials at the Science website.* .

34. A. Butz, S. Guerlet, O. Hasekamp, D. Schepers, A. Galli, I. Aben, C. Frankenberg, J.-M. Hartmann, H. Tran, A. Kuze, G. Keppel-Aleks, G. Toon, D. Wunch, P. Wennberg, N. Deutscher, D. Griffith, R. Macatangay, J. Messerschmidt, J. Notholt, T. Warneke, Toward accurate CO₂ and CH₄ observations from GOSAT. *Geophys. Res. Lett.* **38**, n/a-n/a (2011), doi:10.1029/2011GL047888.

35. T. E. Taylor, C. W. O'Dell, D. Crisp, A. Kuze, H. Lindqvist, P. O. Wennberg, A. Chatterjee, M. Gunson, A. Eldering, B. Fisher, M. Kiel, R. R. Nelson, A. Merrelli, G. Osterman, F. Chevallier, P. I. Palmer, L. Feng, N. M. Deutscher, M. K. Dubey, D. G. Feist, O. E. García, D. W. T. Griffith, F. Hase, L. T. Iraci, R. Kivi, C. Liu, M. de Mazière, I. Morino, J. Notholt, Y.-S. Oh, H. Ohyama, D. F. Pollard, M. Rettinger, M. Schneider, C. M. Roehl, M. K. Sha, K. Shiomi, K. Strong, R. Sussmann, Y. Té, V. A. Velazco, M. Vrekoussis, T. Warneke, D. Wunch, An 11-year record of XCO₂ estimates derived from GOSAT measurements using the NASA ACOS version 9 retrieval algorithm. *Earth Syst. Sci. Data.* **14**, 325–360 (2022), doi:10.5194/essd-14-325-2022.

36. A. Eldering, P. O. Wennberg, D. Crisp, D. S. Schimel, M. R. Gunson, A. Chatterjee, J. Liu, F. M. Schwandner, Y. Sun, C. W. O'Dell, C. Frankenberg, T. Taylor, B. Fisher, G. B. Osterman, D. Wunch, J. Hakkarainen, J. Tamminen, B. Weir, The Orbiting Carbon Observatory-2 early science investigations of regional carbon dioxide fluxes. *Science.* **358**, eaam5745 (2017), doi:10.1126/science.aam5745.

37. Y. Villalobos, P. J. Rayner, J. D. Silver, S. Thomas, V. Haverd, J. Knauer, Z. M. Loh, N. M. Deutscher, D. W. T. Griffith, D. F. Pollard, Interannual variability in the Australian carbon

cycle over 2015–2019, based on assimilation of OCO-2 satellite data. *Atmospheric Chemistry and Physics Discussions*, 1–57 (2022), doi:10.5194/acp-2022-15.

38. D. Wunch, G. C. Toon, J.-F. L. Blavier, R. A. Washenfelder, J. Notholt, B. J. Connor, D. W. T. Griffith, V. Sherlock, P. O. Wennberg, The Total Carbon Column Observing Network. *Phil. Trans. R. Soc. A*. **369**, 2087–2112 (2011), doi:10.1098/rsta.2010.0240.

39. W. Peters, A. R. Jacobson, C. Sweeney, A. E. Andrews, T. J. Conway, K. Masarie, J. B. Miller, L. M. P. Bruhwiler, G. Pétron, A. I. Hirsch, D. E. J. Worthy, G. R. van der Werf, J. T. Randerson, P. O. Wennberg, M. C. Krol, P. P. Tans, An atmospheric perspective on North American carbon dioxide exchange: CarbonTracker. *Proc. Natl. Acad. Sci. USA*. **104**, 18925–18930 (2007), doi:10.1073/pnas.0708986104.

40. F. Chevallier, P. Ciais, T. J. Conway, T. Aalto, B. E. Anderson, P. Bousquet, E. G. Brunke, L. Ciattaglia, Y. Esaki, M. Fröhlich, CO₂ surface fluxes at grid point scale estimated from a global 21 year reanalysis of atmospheric measurements. *J. Geophys. Res. Atmos.* **115** (2010).

41. S. Basu, S. Guerlet, A. Butz, S. Houweling, O. Hasekamp, I. Aben, P. Krummel, P. Steele, R. Langenfelds, M. Torn, S. Biraud, B. Stephens, A. Andrews, D. Worthy, Global CO₂ fluxes estimated from GOSAT retrievals of total column CO₂. *Atmos. Chem. Phys.* **13**, 8695–8717 (2013), doi:10.5194/acp-13-8695-2013.

42. S. Sitch, P. Friedlingstein, N. Gruber, S. D. Jones, G. Murray-Tortarolo, A. Ahlström, S. C. Doney, H. Graven, C. Heinze, C. Huntingford, S. Levis, P. E. Levy, M. Lomas, B. Poulter, N. Viovy, S. Zaehle, N. Zeng, A. Arneth, G. Bonan, L. Bopp, J. G. Canadell, F. Chevallier, P. Ciais, R. Ellis, M. Gloor, P. Peylin, S. L. Piao, C. Le Quéré, B. Smith, Z. Zhu, R. Myneni, Recent trends and drivers of regional sources and sinks of carbon dioxide. *Biogeosciences*. **12**, 653–679 (2015), doi:10.5194/bg-12-653-2015.

43. S. Besnard, N. Carvalhais, M. A. Arain, A. Black, B. Brede, N. Buchmann, J. Chen, J. G. P. W. Clevers, L. P. Dutrieux, F. Gans, M. Herold, M. Jung, Y. Kosugi, A. Knohl, B. E. Law, E. Paul-Limoges, A. Lohila, L. Merbold, O. Roupsard, R. Valentini, S. Wolf, X. Zhang, M. Reichstein, Memory effects of climate and vegetation affecting net ecosystem CO₂ fluxes in
5 global forests. *PloS one*. **14**, e0211510 (2019), doi:10.1371/journal.pone.0211510.
44. T. E. Huxman, K. A. Snyder, D. Tissue, A. J. Leffler, K. Ogle, W. T. Pockman, D. R. Sandquist, D. L. Potts, S. Schwinning, Precipitation pulses and carbon fluxes in semiarid and arid ecosystems. *Oecologia*. **141**, 254–268 (2004).
45. F. E. Moyano, S. Manzoni, C. Chenu, Responses of soil heterotrophic respiration to moisture
10 availability: An exploration of processes and models. *Soil Biology and Biochemistry*. **59**, 72–85 (2013), doi:10.1016/j.soilbio.2013.01.002.
46. W. BORKEN, E. MATZNER, Reappraisal of drying and wetting effects on C and N mineralization and fluxes in soils. *Glob Change Biol*. **15**, 808–824 (2009),
doi:10.1111/j.1365-2486.2008.01681.x.
- 15 47. J. P. Schimel, Life in Dry Soils: Effects of Drought on Soil Microbial Communities and Processes. *Annu. Rev. Ecol. Evol. Syst*. **49**, 409–432 (2018), doi:10.1146/annurev-ecolsys-110617-062614.
48. K. R. Gurney, R. M. Law, A. S. Denning, P. J. Rayner, B. C. Pak, D. Baker, P. Bousquet, L. Bruhwiler, Y.-H. Chen, P. Ciais, I. Y. Fung, M. Heimann, J. John, T. Maki, S. Maksyutov, P.
20 Peylin, M. Prather, S. Taguchi, Transcom 3 inversion intercomparison: Model mean results for the estimation of seasonal carbon sources and sinks. *Global Biogeochem. Cycles*. **18**, n/a–n/a (2004), doi:10.1029/2003GB002111.

49. Science Data Operations System Jet Propulsion Laboratory, “ACOS GOSAT/TANSO-FTS Level 2 bias-corrected XCO₂ and other select fields from the full-physics retrieval aggregated as daily files V9r”. (2020).
50. Science Data Operations System, Jet Propulsion Laboratory, “OCO-2 Level 2 bias-corrected XCO₂ and other select fields from the full-physics retrieval aggregated as daily files, Retrospective processing V10r”. (2020).
51. A. R. Jacobson *et al.*, *CarbonTracker CT2019B* (NOAA Global Monitoring Laboratory, 2020) (available at <https://www.esrl.noaa.gov/gmd/ccgg/carbontracker/CT2019B/>).
52. F. Chevallier, R. J. Engelen, P. Peylin, The contribution of AIRS data to the estimation of CO₂ sources and sinks. *Geophys. Res. Lett.* **32**, L23801 (2005).
53. F. Chevallier, M. Remaud, C. W. O’Dell, D. Baker, P. Peylin, A. Cozic, Objective evaluation of surface- and satellite-driven carbon dioxide atmospheric inversions. *Atmos. Chem. Phys.* **19**, 14233–14251 (2019), doi:10.5194/acp-19-14233-2019.
54. K. A. Masarie, W. Peters, A. R. Jacobson, P. P. Tans, ObsPack: a framework for the preparation, delivery, and attribution of atmospheric greenhouse gas measurements. *Earth Syst. Sci. Data.* **6**, 375–384 (2014), doi:10.5194/essd-6-375-2014.
55. NOAA, *Global Monitoring Laboratory: Trends in Atmospheric Carbon Dioxide* (available at https://www.esrl.noaa.gov/gmd/ccgg/trends/gl_gr.html).
56. Anton S. Darmenov, Arlindo da Silva, in *Technical Report Series on Global Modeling and Data Assimilation, Volume 38* .
57. T. Oda, S. Maksyutov, A very high-resolution (1 km×1 km) global fossil fuel CO₂ emission inventory derived using a point source database and satellite observations of nighttime lights. *Atmos. Chem. Phys.* **11**, 543–556 (2011), doi:10.5194/acp-11-543-2011.

58. T. Oda, S. Maksyutov, R. J. Andres, The Open-source Data Inventory for Anthropogenic Carbon dioxide (CO₂), version 2016 (ODIAC2016): A global, monthly fossil-fuel CO₂ gridded emission data product for tracer transport simulations and surface flux inversions. *Earth Syst. Sci. Data*. **10**, 87–107 (2018), doi:10.5194/essd-10-87-2018.
- 5 59. B. Weir, L. E. Ott, G. J. Collatz, S. R. Kawa, B. Poulter, A. Chatterjee, T. Oda, S. Pawson, Bias-correcting carbon fluxes derived from land-surface satellite data for retrospective and near-real-time assimilation systems. *Atmos. Chem. Phys.* **21**, 9609–9628 (2021), doi:10.5194/acp-21-9609-2021.
- 10 60. J. T. Randerson, M. V. Thompson, C. M. Malmstrom, C. B. Field, I. Y. Fung, Substrate limitations for heterotrophs: Implications for models that estimate the seasonal cycle of atmospheric CO₂. *Global Biogeochem. Cycles*. **10**, 585–602 (1996), doi:10.1029/96GB01981.
- 15 61. J. Muñoz Sabater, ERA5-Land monthly averaged data from 1981 to present. *Copernicus Climate Change Service (C3S) Climate Data Store (CDS)*, Accessed on 20.12.2021 (2019), doi:10.24381/cds.68d2bb3.
62. J. Muñoz Sabater, ERA5-Land monthly averaged data from 1981 to present. *Copernicus Climate Change Service (C3S) Climate Data Store (CDS)*, Accessed on 20.12.2021 (2021), doi:10.24381/cds.68d2bb3.
- 20 63. D. W. Griffith *et al.*, *TCCON data from Darwin (AU), Release GGG2014.R0* (CaltechDATA, 2014) (available at <https://data.caltech.edu/records/269>).
64. Griffith, D. W. T., Velazco, V. A., Deutscher, N. M., Paton-Walsh, C., Jones, N. B., Wilson, S. R., Macatangay, R. C., Kettlewell, G. C., Buchholz, R. R., & Rigggenbach, M. O., *TCCON data from Wollongong (AU), Release GGG2014.R0 (Version GGG2014.R0) [Data set]* (2014).

65. F. Di Giuseppe, S. Rémy, F. Pappenberger, F. Wetterhall, *Combining fire radiative power observations with the fire weather index improves the estimation of fire emissions* (2017).
66. C. Wiedinmyer, S. K. Akagi, R. J. Yokelson, L. K. Emmons, J. A. Al-Saadi, J. J. Orlando, A. J. Soja, The Fire INventory from NCAR (FINN) – a high resolution global model to estimate the emissions from open burning. *Geosci. Model Dev.* **4**, 625–641 (2011), doi:10.5194/gmdd-3-2439-2010.
67. Jason Beringer, *Daly Uncleared OzFlux tower site OzFlux: Australian and New Zealand Flux Research and Monitoring* (2013) (available at <https://doi.org/10.21955/ozflux.daly>).
68. Jason Beringer, *Dry River OzFlux tower site OzFlux: Australian and New Zealand Flux Research and Monitoring* (2013) (available at <https://doi.org/10.21955/ozflux.dryriver>).
69. James Cleverly, *Alice Springs Mulga OzFlux site OzFlux: Australian and New Zealand Flux Research and Monitoring* (2011) (available at <https://doi.org/10.21955/ozflux.alicesprings>).
70. OCO-2 Science Team, Michael Gunson, Annmarie Eldering, “ACOS GOSAT/TANSO-FTS Level 2 Full Physics Standard Product V9r”.
71. OCO-2 Science Team, Michael Gunson, Annmarie Eldering, “OCO-2 Level 2 bias-corrected XCO₂ and other select fields from the full-physics retrieval aggregated as daily files, Retrospective processing V10r”.
72. G. R. van der Werf, J. T. Randerson, L. Giglio, T. T. van Leeuwen, Y. Chen, B. M. Rogers, M. Mu, M. J. E. van Marle, D. C. Morton, G. J. COLLATZ, R. J. Yokelson, P. S. Kasibhatla, Global fire emissions estimates during 1997–2016. *Earth Syst. Sci. Data.* **9**, 697–720 (2017), doi:10.5194/essd-9-697-2017.
73. C. H. Reick, V. Gayler, D. Goll, S. Hagemann, M. Heidkamp, J. E. M. S. Nabel, T. Raddatz, E. Roeckner, R. Schnur, S. Wilkenskjaeld, “JSBACH 3 - The land component of the MPI Earth System Model: documentation of version 3.2”. (2021).

74. J. R. Melton, V. K. Arora, E. Wisernig-Cojoc, C. Seiler, M. Fortier, E. Chan, L. Teckentrup, CLASSIC v1.0: the open-source community successor to the Canadian Land Surface Scheme (CLASS) and the Canadian Terrestrial Ecosystem Model (CTEM) – Part 1: Model framework and site-level performance. *Geosci. Model Dev.* **13**, 2825–2850 (2020), doi:10.5194/gmd-13-2825-2020.
75. B. Poulter, P. Ciais, E. Hodson, H. Lischke, F. Maignan, S. Plummer, N. E. Zimmermann, Plant functional type mapping for earth system models. *Geosci. Model Dev.* **4**, 993–1010 (2011), doi:10.5194/gmd-4-993-2011.
76. X. Yue, N. Unger, The Yale Interactive terrestrial Biosphere model version 1.0: description, evaluation and implementation into NASA GISS ModelE2. *Geosci. Model Dev.* **8**, 2399–2417 (2015), doi:10.5194/gmd-8-2399-2015.
77. S. Zaehle, A. D. Friend, P. Friedlingstein, F. Dentener, P. Peylin, M. Schulz, Carbon and nitrogen cycle dynamics in the O-CN land surface model: 2. Role of the nitrogen cycle in the historical terrestrial carbon balance. *Global Biogeochem. Cycles.* **24**, n/a-n/a (2010), doi:10.1029/2009GB003522.
78. D. S. Goll, E. Joetzjer, M. Huang, P. Ciais, Low Phosphorus Availability Decreases Susceptibility of Tropical Primary Productivity to Droughts. *Geophys. Res. Lett.* **45**, 8231–8240 (2018), doi:10.1029/2018GL077736.
79. G. Krinner, N. Viovy, N. de Noblet-Ducoudré, J. Ogée, J. Polcher, P. Friedlingstein, P. Ciais, S. Sitch, I. C. Prentice, A dynamic global vegetation model for studies of the coupled atmosphere-biosphere system. *Global Biogeochem. Cycles.* **19** (2005), doi:10.1029/2003GB002199.
80. N. Vuichard, P. Messina, S. Luyssaert, B. Guenet, S. Zaehle, J. Ghattas, V. Bastrikov, P. Peylin, Accounting for carbon and nitrogen interactions in the global terrestrial ecosystem

model ORCHIDEE (trunk version, rev 4999): multi-scale evaluation of gross primary production. *Geosci. Model Dev.* **12**, 4751–4779 (2019), doi:10.5194/gmd-12-4751-2019.

81. V. Haverd, B. Smith, L. Nieradzick, P. R. Briggs, W. Woodgate, C. M. Trudinger, J. G. Canadell, M. Cuntz, A new version of the CABLE land surface model (Subversion revision r4601) incorporating land use and land cover change, woody vegetation demography, and a novel optimisation-based approach to plant coordination of photosynthesis. *Geosci. Model Dev.* **11**, 2995–3026 (2018), doi:10.5194/gmd-11-2995-2018.
82. D. M. Lawrence, R. A. Fisher, C. D. Koven, K. W. Oleson, S. C. Swenson, G. Bonan, N. Collier, B. Ghimire, L. Kampenhout, D. Kennedy, E. Kluzek, P. J. Lawrence, F. Li, H. Li, D. Lombardozzi, W. J. Riley, W. J. Sacks, M. Shi, M. Vertenstein, W. R. Wieder, C. Xu, A. A. Ali, A. M. Badger, G. Bisht, M. Broeke, M. A. Brunke, S. P. Burns, J. Buzan, M. Clark, A. Craig, K. Dahlin, B. Drewniak, J. B. Fisher, M. Flanner, A. M. Fox, P. Gentine, F. Hoffman, G. Keppel-Aleks, R. Knox, S. Kumar, J. Lenaerts, L. R. Leung, W. H. Lipscomb, Y. Lu, A. Pandey, J. D. Pelletier, J. Perket, J. T. Randerson, D. M. Ricciuto, B. M. Sanderson, A. Slater, Z. M. Subin, J. Tang, R. Q. Thomas, M. Val Martin, X. Zeng, The Community Land Model Version 5: Description of New Features, Benchmarking, and Impact of Forcing Uncertainty. *J. Adv. Model. Earth Syst.* **11**, 4245–4287 (2019), doi:10.1029/2018MS001583.
83. H. Tian, G. Chen, C. Lu, X. Xu, D. J. Hayes, W. Ren, S. Pan, D. N. Huntzinger, S. C. Wofsy, North American terrestrial CO₂ uptake largely offset by CH₄ and N₂O emissions: toward a full accounting of the greenhouse gas budget. *Climatic change.* **129**, 413–426 (2015), doi:10.1007/s10584-014-1072-9.
84. W. Yuan, D. Liu, W. Dong, S. Liu, G. Zhou, G. Yu, T. Zhao, J. Feng, Z. Ma, J. Chen, Y. Chen, S. Chen, S. Han, J. Huang, L. Li, H. Liu, S. Liu, M. Ma, Y. Wang, J. Xia, W. Xu, Q. Zhang, X. Zhao, L. Zhao, Multiyear precipitation reduction strongly decreases carbon uptake

over northern China. *J. Geophys. Res. Biogeosci.* **119**, 881–896 (2014),
doi:10.1002/2014JG002608.

85. P. Meiyappan, A. K. Jain, J. I. House, Increased influence of nitrogen limitation on CO₂
emissions from future land use and land use change. *Global Biogeochem. Cycles.* **29**, 1524–
5 1548 (2015), doi:10.1002/2015GB005086.

86. C. Delire, R. Séférian, B. Decharme, R. Alkama, J.-C. Calvet, D. Carrer, A.-L. Gibelin, E.
Joetzjer, X. Morel, M. Rocher, D. Tzanos, The Global Land Carbon Cycle Simulated With
ISBA-CTRIP: Improvements Over the Last Decade. *J. Adv. Model. Earth Syst.* **12** (2020),
doi:10.1029/2019MS001886.

10 87. A. A. Sellar, C. G. Jones, J. P. Mulcahy, Y. Tang, A. Yool, A. Wiltshire, F. M. O’connor, M.
Stringer, R. Hill, J. Palmieri, others, UKESM1: Description and evaluation of the UK Earth
System Model. *J. Adv. Model. Earth Syst.* **11**, 4513–4558 (2019).

88. S. Lienert, F. Joos, A Bayesian ensemble data assimilation to constrain model parameters and
land-use carbon emissions. *Biogeosciences.* **15**, 2909–2930 (2018), doi:10.5194/bg-15-2909-
15 2018.

89. A. P. Walker, T. Quaipe, P. M. van Bodegom, M. G. de Kauwe, T. F. Keenan, J. Joiner, M.
R. Lomas, N. MacBean, C. Xu, X. Yang, F. I. Woodward, The impact of alternative trait-
scaling hypotheses for the maximum photosynthetic carboxylation rate (V_{cmax}) on global
gross primary production. *The New phytologist.* **215**, 1370–1386 (2017),
20 doi:10.1111/nph.14623.

90. E. Kato, T. Kinoshita, A. Ito, M. Kawamiya, Y. Yamagata, Evaluation of spatially explicit
emission scenario of land-use change and biomass burning using a process-based
biogeochemical model. *Journal of Land Use Science.* **8**, 104–122 (2013),
doi:10.1080/1747423x.2011.628705.

Acknowledgments: We thank the Japanese Aerospace Exploration Agency, National Institute for Environmental Studies and the Ministry of Environment for the GOSAT data and their continuous support as part of the Joint Research Agreement. OCO-2 data were produced by the OCO-2 project at the Jet Propulsion Laboratory, California Institute of Technology, and obtained from the OCO-2 data archive maintained at the NASA Goddard Earth Science Data and Information Services Center. CarbonTracker CT2019B results are provided by NOAA ESRL, Boulder, Colorado, USA from the website at <http://carbontracker.noaa.gov>. We thank all TRENDY modelers for providing model output as part of the TRENDY v9 ensemble. The study has greatly benefited from discussions with Christian Frankenberg.

Author contributions:

AB, SNV, and EMM were involved in conceptualization and methodology. EMM conducted the formal analysis and the visualization under supervision of AB and SNV. AB, SNV, EMM, MJ, and SB wrote the original draft. SB performed the dedicated TM5-4DVar runs. SS, VKA, PRB, PF, DSG, AKJ, EK, JEMSN, BP, RS, HT, AW, WY, XY, SZ provided TRENDY data. NMD and DWTG provided TCCON data. All authors contributed to the editing and review of the manuscript.

Competing interests: Authors declare that they have no competing interests.

Data and materials availability: GOSAT/RemoTeC2.4.0 XCO₂ data can be obtained from doi: 10.5281/zenodo.5886662 (last access: 2022-02-25). GOSAT/ACOS data is available at https://oco2.gesdisc.eosdis.nasa.gov/data/GOSAT_TANSO_Level2/ACOS_L2_Lite_FP_9r/ (last access: 2020-07-28). OCO-2 data is available at https://disc.gsfc.nasa.gov/datasets/OCO2_L2_Lite_FP_10r/summary (last access: 2020-11-01). TCCON data can be downloaded at <https://data.caltech.edu/records/269> (last access: 2022-02-25). CarbonTracker CT2019B CO₂ fluxes and concentrations can be downloaded from <https://gml.noaa.gov/aftp/products/carbontracker/co2/CT2019B/fluxes/monthly/> (last access: 2021-02-19) and https://gml.noaa.gov/aftp/products/carbontracker/co2/CT2019B/molefractions/co2_total_monthly/ (last access: 2022-02-25) respectively. CAMS concentrations and fluxes can be found at datasets/data/cams-ghg-inversions/ (last access: 2021-10-07). GFAS emissions records are available at <https://apps.ecmwf.int/datasets/data/cams-gfas/> (last access: 2020-11-13). CAMS and GFAS data were generated using Copernicus Atmosphere Service Information [2021] and neither the European Commission nor ECMWF is responsible for any use that may be made of the information it contains. GFED fire emissions are available at <https://www.geo.vu.nl/~gwerf/GFED/GFED4/> (last access: 2020-07-10). FINN data were retrieved from the American National Center for Atmospheric Research <https://www2.acom.ucar.edu/modeling/finn-fire-inventory-ncar> (last access: 2020-11-18). The used OzFlux data can be downloaded from <https://www.ozflux.org.au/> (last access: 2021-11-16). ERA5-land data records contain modified Copernicus Atmosphere Service Information [2021] available at the Climate Data Store <https://cds.climate.copernicus.eu/cdsapp#!/dataset/reanalysis-era5-land-monthly-means> (last access: 2021-12-20). TRENDYv9 model output and FLUXCOM products are available upon

request (<https://sites.exeter.ac.uk/trendy> and <http://fluxcom.org/CF-Download/> respectively).
The TM5-4DVar data can be requested from the corresponding authors.

The code used in this study is available from the corresponding authors on reasonable request.

5 **Supplementary Materials:**

Materials and Methods

Figs. S1 to S7

Tables S1 to S2

References (48-90)

10